Relaxation dynamics of semiflexible treelike small-world polymer networks

Edieliton S. Oliveira
Departamento de Fisica, Universidade Federal do Amazonas, 69077-000 Manaus, Brazil

Ana Célia A. M. Galiceanu
Universidade Federal do Amazonas, 69077-000 Manaus, Brazil

Aurel Jurjiu[*]
Faculty of Physics, Babes-Bolyai University, Street Mihail Kogalniceanu 1, 400084 Cluj-Napoca, Romania

Mircea Galiceanu[†]
Departamento de Física, Universidade Federal do Amazonas, 69077-000 Manaus, Brazil

(Received 6 February 2019; published 14 August 2019)

We study the relaxation dynamics of the polymer networks that are constructed based on a degree distribution specific to small-world networks. The employed building algorithm generates polymers with a large variety of architectures, thus allowing for a detailed study of the structural transition from a pure linear chain to dendritic polymer networks. This is done by varying a single parameter p, which measures the randomness in the degree of the network's nodes. The dynamics is investigated in the framework of the generalized Gaussian structures model by monitoring the influence of the parameter p and of the stiffness parameter q on the behavior of the relaxation quantities: averaged monomer displacement, storage modulus, and loss modulus. The structure properties of the constructed polymers are described by the mean-square radius of gyration. In the absence of stiffness, in the intermediate frequencies domain of the dynamical quantities we encounter different behaviours, such as a dendritic behavior followed by a linear one for very small values of p or a single well-marked dendritic behavior for higher values of p. The stiffness parameter q influences drastically the relaxation dynamics of these polymer networks and in general no evident scaling regions were encountered. However, for some values of the parameter set (p, q), such as $(0.8, 0.4)$, an extremely short constant slope region, less than one order of magnitude, was found.

DOI: 10.1103/PhysRevE.100.022501

I. INTRODUCTION

Small-world network is the first well-succeeded model that explains some peculiar properties of real complex networks, such as technological, economic, and transport networks [1–5], chemical-reaction networks [6], protein-protein interaction networks [7,8], protein residue network [9], genetic networks [10–12], brain networks [13–15], food webs [16–19], social networks [20–22], and computer networks [23,24]. While the first theoretical model of small-world networks was introduced by Watts and Strogatz [25], in the recent years, given their relevance for diverse realistic situations, many other theoretical models or variants have been developed [26–30]. These networks share the same topological property: the diameter grows logarithmically with the size of the network [31], which means that the distances between any nodes keep *small*. Here the diameter is defined as the largest distance between two nodes calculated in terms of links connecting them. In the present study we use an algorithm [32] that creates treelike networks starting from a Poisson-like degree distribution, which is one of the main consequence of the *small-world* effect. Based on this algorithm, the degree of each node, i.e., the number of its nearest neighbors, is randomly chosen from the degree distribution of the initial Watts-Strogatz small-world model [25]. We set the value of the minimum allowed degree equal to two, ensuring that during the growing process all the newly created nodes have at least one open link and the construction of the networks will never stop by itself, but only when the desired size is reached. At this point all open nodes, i.e., peripheral nodes, receive the degree one and the construction algorithm stops. Our model enables us to monitor in details the transition from a linear chain to a disordered dendritic-like or hyperbranched structure by changing the value of a single parameter. It is important to stress that many scale-free network models show small-world behavior, namely, the diameter remains very small when the network's size increases [31]. One of the most important topological difference between small-world networks and scale-free networks is that the later exhibit hubs, which are nodes with very high degree.

Given the relatively straightforward manner, offered by the Gaussian models, by which many measurable relaxation forms are related by the set of eigenmodes of the system, we choose to perform our study in the framework of the

[*]aurel.jurjiu@phys.ubbcluj.ro
[†]mircea@ufam.edu.br

generalized Gaussian structures (GGS) model [33–38], employing the Rouse-type approach [39]. Being the natural extension of the classical Rouse-Zimm chain models [39,40] to incorporate polymers with complex architectures, the GGS model has been successfully used for describing the dynamics of various flexible polymer systems, such as dendrimers and their derivates [36,41–44], star polymers [36,45], hyperbranched polymers [46–48], fractal polymer networks [49,50], small-world polymer networks [26,32,34,51], scale-free polymer networks [52,53], multihierarchical and multilayered polymer networks [54–59], and comb-of-comb polymer networks [60].

The GGS model inherits all the limitations of its predecessors; it does not account for the excluded volume interactions, the entanglement constraints, and the stiffness effects. It is worth mentioning that, for dry polymer networks and polymer melts the excluded volume effects are rather screened. Regarding the entanglement effects, they are negligible for polymer networks with short network strands between the cross-link points, as it is the case of our networks. However, in the literature there are known models which account for at least one of the aforementioned effects. In this article we continue this research quest by introducing the stiffness effects in the manner of Refs. [33,61–63] to small-world networks constructed from a degree distribution. The inclusion of stiffness effects is motivated by the fact that they influence considerably the dynamics of many biological macromolecules [64–66], such as proteins or DNA. It has been shown that excluded volume acts on local scales as an effective bending rigidity because of the exclusion of large bending angles [67]. In a very general fashion, the stiffness effects are taken into account by fixing the angles between nearest-neighboring bonds and the orientations between all other bonds are found by assuming that the bonds are freely rotating. The imposed restrictions recover the basic properties related to semiflexibility of polymers and many theoretical models use them as their basic foundation [33,61–63,68–75]. Consequently, these new considerations will increase the number of non-vanishing elements of the dynamical matrix of semiflexible polymers in comparison with the fully flexible polymers case. However, also in this case, based on numerical and sometimes analytical methods, one can determine the whole eigenvalue spectrum of the dynamical matrix, which allows to solve the dynamics of semiflexible polymer networks. For describing the mechanical relaxation of the semiflexible treelike small-world polymer structures we analyze the dynamical behaviors of the average monomer displacement and of the storage and loss moduli, while for the structure properties we investigate the behavior of their mean-square radius of gyration.

The use of the aforementioned construction algorithm leads to the obtaining of structures whose geometries range from pure linear chains to branched and hyperbranched networks. In this respect, the present work centers on two fundamental issues in polymer science, how the geometry of the polymer influences its dynamics and the synthesis of macromolecules with controlled topologies. Regarding the relationship between polymer geometry and its dynamics, we monitor the smooth transition from pure chain systems to branched and hyperbranched networks and highlight how this transition is reflected by the dynamical behaviors of different relaxation quantities. The control of the topology is achieved through the parameter set which allows us to predict the type of the obtained structure.

II. CONSTRUCTION MODEL

In this section we briefly present our algorithm which builds treelike networks starting from a degree distribution specific to small-world networks. Our model maintains the basic features of other small-world network models, but, in contrast to the others, it returns treelike structures. Our motivation resides in the fact that to develop theoretical models for hyperbranched polymers the employed building algorithm must create only treelike networks. However, it is worth mentioning that experimentally a transition between networks with loops and treelike networks could be realized [76,77] and the degree of the nodes keeps unaltered during such experiments. All small-world network models lead to a degree distribution having a Poisson function [26,27,31,32]:

$$p_k = e^{-2p}\frac{(2p)^{k-2}}{(k-2)!}, \tag{1}$$

which is valid for $k \geqslant 2$, while $p_1 = 0$. In Eq. (1) we denoted with p_k the probability that a node has k links. The parameter p measures the randomness of the network, having values between 0.0, which corresponds to a regular network (a ring or a line for example) and 1.0, which corresponds to a complete random network. The form of Eq. (1) provides good hints regarding the topology of the resulting network. For low values of p, more precisely for $p < 0.5$, the most frequent degree in the network is 2, i.e., we have a predominantly linearlike topology. For $p = 0.5$ the degrees 2 and 3 have the highest probability to occur, while for $p = 1.0$ one gets the degrees 3 and 4 as the most probable, resulting random hyperbranched structures with short strands between the cross-link points. One can conclude from Eq. (1) that an increase of parameter p leads to the obtaining of a broader distribution of the degrees and the nodes with higher degrees will appear more often. For more details concerning these points the reader is advised to consult the discussion of Fig. 1 in Ref. [32].

In this paper we construct our networks in a treelike fashion with the degree distribution given by Eq. (1) and following in-depth the procedure of Ref. [32]. The building algorithm of a small-world network consisting of $N = 50$ nodes and $p = 0.5$ is displayed in Fig. 1. The numbers displayed in the figure correspond to the chronological order in which the nodes were created. Our algorithm can be resumed as: (i) Create the first node, choose at random its degree k_1 from Eq. (1) and link k_1 new nodes to node 1; (ii) Select randomly an open node α, choose at random its degree k_α from Eq. (1) and link $k_\alpha - 1$ new nodes to node α. The last step is iterated until we obtain a network with N nodes. It is important to stress that the construction of every realization does not stop by itself for lack of open nodes. The constructed networks will be called as *treelike Small-World Networks* and in Fig. 1 we emphasize the treelike aspect of the network by displaying it as a dendritic structure. Nodes from the same generation are depicted by the same color.

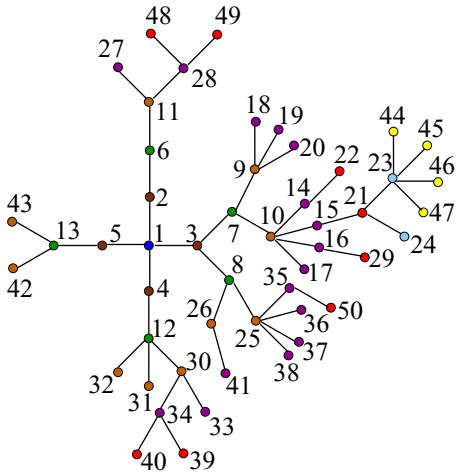

FIG. 1. Example of treelike small-world network constructed from the degree distribution, Eq. (1), having $N = 50$ nodes and $p = 0.5$.

III. THEORETICAL MODEL

In this section, we present the basic concepts of the semiflexible treelike polymers (STPs) model employed in this study and summarize the main formulas concerning the relaxation patterns. For more details concerning the model one can follow the Appendix A and the references within. The dynamics of semiflexible polymer network of N beads having the position vectors $\mathbf{R}_i$ $(i = 1, 2, \ldots, N)$ is described by the Langevin equations, which for the Y component of the position vector $\mathbf{R}_i = \{X_i, Y_i, Z_i\}$ can be written as [34,36,48,52]

$$\zeta \frac{\partial Y_i(t)}{\partial t} + \frac{\partial V_{\mathrm{STP}}(\{\mathbf{R}_k\})}{\partial Y_i} = \tilde{f}_i(t), \tag{2}$$

where $\tilde{f}_i$ is the Y component of the stochastic force acting on the ith bead, ζ denotes the friction coefficient, and $V_{\mathrm{STP}}(\{\mathbf{R}_k\})$ is the potential which accounts for the connections between beads and for the semiflexibility effects. The potential energy V_{STP} is harmonic and can be written as $V_{\mathrm{STP}}(\{\mathbf{R}_k\}) = \frac{K}{2}\sum_{i,j=1}^{N} A_{ij}^{\mathrm{STP}} \mathbf{R}_i \cdot \mathbf{R}_j$, where K is the elasticity constant and A^{STP} is the dynamical matrix. All nonvanishing elements of the matrix A^{STP} can be written in term of the stiffness parameter, q, as shown in details in Appendix A.

The monomer displacement, averaged over the fluctuating forces and over all positions of monomers, is given by [33,36]

$$\langle\langle Y \rangle\rangle = \frac{t}{N} + \frac{1}{N}\sum_{n=2}^{N} \frac{1 - \exp(-\lambda_n t)}{\lambda_n}, \tag{3}$$

where λ_n are the eigenvalues of $\mathbf{A}^{\mathrm{STP}}$. The last equation is identical with Eq. (A9) from Appendix A, for a proper choice of the constants.

Apart from $\langle\langle Y \rangle\rangle$, a quantity which may be accessed through micromechanical manipulations, classical experiments focus on the mechanical and dielectric relaxation. An experimentally readily accessible quantity is the complex dynamic modulus, $G^*(\omega)$, which is usually determined by applying an external harmonic strain to the system. Even more familiar are the storage $G'(\omega)$ and the loss $G''(\omega)$ moduli [78–81], which represent the real and the imaginary components of $G^*(\omega)$.

For very dilute solutions and for $\omega > 0$ the storage and loss moduli in the Rouse-type formalism are given by

$$G'(\omega) = \nu k_B T \frac{1}{N}\sum_{n=2}^{N} \frac{\omega^2}{\omega^2 + (2\sigma\lambda_n)^2} \tag{4}$$

and

$$G''(\omega) = \nu k_B T \frac{1}{N}\sum_{n=2}^{N} \frac{2\sigma\omega\lambda_n}{\omega^2 + (2\sigma\lambda_n)^2}. \tag{5}$$

In Eqs. (4) and (5), ν is the number of polymer segments (beads) per unit volume and λ_n are the eigenvalues of $\mathbf{A}^{\mathrm{STP}}$. In these equations the vanishing eigenvalue ($\lambda_1 = 0$), which corresponds to the translation of the system as a whole, is neglected. Here our main interest is in the scaling or nonscaling behavior of the relaxation moduli, thus we choose to display the results in terms of the reduced storage and loss moduli by setting $\nu k_B T/N = 1$ and the bond rate constant $\sigma = \frac{K}{\zeta} = \frac{3k_B T}{l^2 \zeta} = 1$ in Eqs. (4) and (5), where K_B is the Boltzmann constant, T is the temperature, and l^2 is the mean-square length for each bond vector.

IV. RESULTS

In this section we present the results obtained for the semiflexible treelike small-world polymer networks (SSWNs) which were built by using the degree distribution given by Eq. (1). Naturally, these networks depend on two parameters: the number of nodes, N, and the randomness parameter, p, which appears in the considered degree distribution, Eq. (1). The theoretical model for the relaxation dynamics introduces additionally the stiffness parameter, q. Given the fact that the overall procedure of creating the networks deals with randomness, all structure and dynamical quantities are averaged over statistical ensembles. In this respect, we have averaged over S different realizations of the algorithm for each parameters' set (N, p, q), in such a way that the product NS is kept constant. This manner ensures an averaging over the same number of eigenvalues, although the size of the networks changes. All results to be presented in this section have been obtained for SSWNs of size $N = 4000$ nodes and averaged over $S = 250$ realizations.

A. Eigenvalue spectrum

In Fig. 2 we analyze the particular impact of each parameter on the eigenvalue spectrum of the matrix $\mathbf{A}^{\mathrm{STP}}$. This analysis is motivated by the dependence of the dynamic [see Eqs. (3)–(5)] and structure quantities (see Appendix B) on the entire eigenvalue spectrum.

A quantity that captures the large scale behavior of the eigenvalues is the spectral density, $n(\lambda)$. Figure 2(a) displays the eigenvalue spectral density of the matrix $\mathbf{A}^{\mathrm{STP}}$ for SSWNs with p fixed to 0.1 and the stiffness parameter varying from 0.0 to 0.8, the first value corresponding to the fully flexible bonds case. Our main focus is the region of small eigenvalues which gives the largest contribution to the dynamical

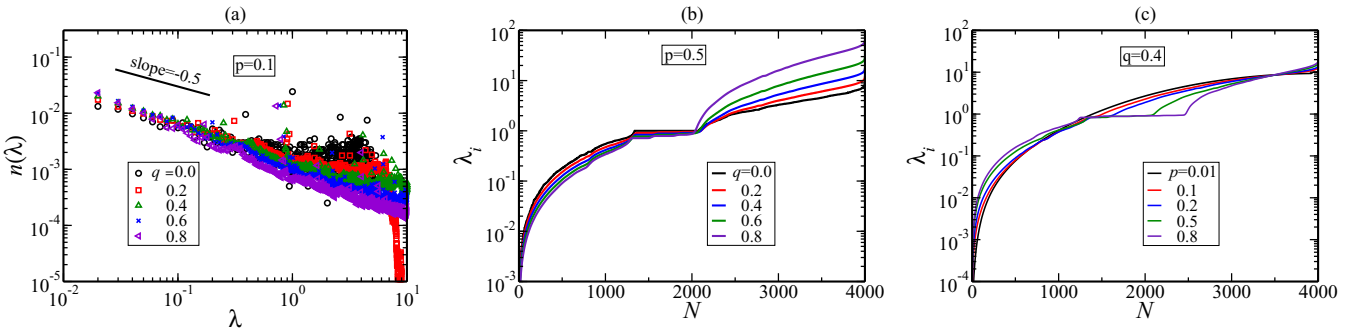

FIG. 2. Eigenvalue spectra for SSWNs with $N = 4000$ nodes and $S = 250$ realizations. Other parameters are: (a) $p = 0.1$ and q is variable, (b) $p = 0.5$ and q is variable, and (c) p is variable and $q = 0.4$.

quantities. Remarkably, in this eigenvalue region the spectral density obeys power-law behavior, $n(\lambda) \sim \lambda^{-\beta}$, regardless of the employed bond stiffness value. Going from fully flexible to very stiff bonds the power-law exponent changes from $\beta = 0.49$ to $\beta = 0.77$; the first value being in good agreement with the theoretical expected value 0.5 for ideal Rouse chains ($p = 0$; $q = 0$), whence one can infer that the networks have linearlike topology. The larger values of β show that the behavior of spectral density deviates strongly from that of an ideal chain when stiffness is considered. Reliable information about the structure topology can be extracted from the particular type of eigenvalue 1. The eigenvalue 1 appears nondegenerate in the spectrum of pure linear chain. In contrast, the eigenvalue 1 appears degenerate in the eigenvalue spectra of dendritic structures and it corresponds to a sequence of beads connected in the starwise fashion. The fact that the eigenvalue 1 appears degenerate highlights the existence of a dendritic component of the achieved networks. Thus, beside the linear chain component, there is also a rather significant number of branched segments and the obtained structures are called chainlike networks. In the eigenvalue spectrum of fully flexible networks we notice the appearance of a "pseudo-gap" right after the eigenvalue 1. It is due to the increase of the degeneracy of eigenvalue 1 caused by the structural transition from pure chain to chain like-networks. The "pseudo-gap" is smoothed away by imposing bond stiffness, as the effect of reducing the matrix sparsity. Figure 2(b) displays the eigenvalues in ascending order for SSWNs with p set to 0.5 and q ranges from 0.0 to 0.8. These networks consist of mixture of short linear segments and dendritic fragments with various functionalities. The influence of bond stiffness on the eigenvalue spectrum manifests mostly at its extremities; with the rise of stiffness parameter, the largest eigenvalues are increasing and the smallest eigenvalues are decreasing. It is worth remarking that the total number of distinct eigenvalues in the semiflexible case is larger than in the flexible one. This is due to the fact that the matrix $\mathbf{A}^{\mathrm{STP}}$ in the semiflexible case is less sparse. The most degenerate eigenvalue is given by $\lambda = f/(f + q)$, where f is the functionality of the node. This expression was also reported for all hyperbranched structures studied in Refs. [33,61,68,69]. When $q = 0$ the expression reduces to $\lambda = 1$, which is the most degenerate eigenvalue in the fully flexible case. Figure 2(c) presents the eigenvalues in ascending order for SSWNs with stiffness parameter set to 0.4 and the randomness parameter extending from 0.01 to 0.8. For very low values of p we obtain networks chiefly composed by linear segments, resulting an eigenvalue spectrum consisting mainly of nondegenerate eigenvalues and, in the same time, the degenerate ones having lower degeneracies. For high values of p we have hyperbranched networks composed by nodes with variable degree, which transform the eigenvalue spectrum into a degenerated one, having the most degenerate eigenvalue equal to $\lambda \approx f/(f + 0.4)$.

B. Mechanical relaxation

We continue the study of the SSWNs by focusing on their mechanical relaxation dynamics. By choosing suitable parameter set values, the impact of bond stiffness on the mechanical relaxation of SSWNs is monitored in the dynamical behavior of the storage modulus, while the influence of the allowed degree of randomness is monitored in the dynamical behavior of the loss modulus. In Fig. 3 we present the results obtained for the storage modulus, $G'(\omega)$, calculated based on Eq. (4) in which we set $\nu k_B T/N = 1$ and $\sigma = 1$. The randomness parameter is fixed to 0.1 in Fig. 3(a) and to 0.5 in Fig. 3(b), while in both Figs. 3(a) and 3(b) the stiffness parameter varies from 0.0 to 0.8. For a better viewing of the dynamical behavior shown by the curves we plot as inset panels their derivatives $\alpha' = \frac{d\log_{10}G'(\omega)}{d\log_{10}\omega}$ in semilogarithmic scale. Evidently from both panels are the limiting connectivity-independent behaviors, namely, for very large frequencies one has $G'(\omega) \sim \omega^0$ meaning single-bead mechanical response, whereas for very small frequencies one finds $G'(\omega) \sim \omega^2$ representing the mechanical response of the entire network. The microscopic characteristics (i.e., the particular topology) of the polymer system reveal only in the intermediate frequency region. Remarkably, the intermediate frequency domain of the curves from Fig. 3(a) highlights explicitly the reflection of the geometry of the constituent parts of the network in the dynamical behavior of the storage modulus. For all employed values of the parameter set, the intermediate frequency domain of the curves decomposes into two regions. In the region located at smaller intermediate frequencies the curves are concave downward which indicates a typical dendriticlike behavior. The curves in the region of larger intermediate frequencies appear as straight lines which, in the double logarithmic scales, denote power-law behavior.

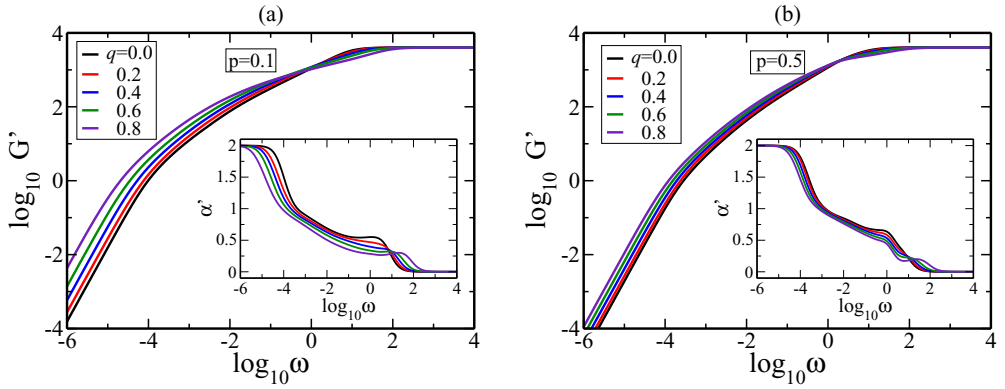

FIG. 3. Storage modulus and its derivative for SSWNs with $N = 4000$ and $S = 250$ realizations. (a) $p = 0.1$ and (b) $p = 0.5$ with the stiffness parameter q being varied.

For the case of fully flexible bonds, the value of the slope in the scaling region is 0.54 which is a trademark of linear chain behavior. For the semiflexible case, the slope of the scaling region corresponding to the relaxation of linear segments decreases with the increase of stiffness, meaning that the rise of bond stiffness slows the relaxation. It is worth mentioning that for $q = 0.6$ and $q = 0.8$ the obtained plateau values $\alpha' \approx 0.32$, respectively $\alpha' \approx 0.26$ are similar with those obtained in Ref. [63] for linear segments and large values of stiffness parameter.

In Fig. 3(b), where $p = 0.5$, the curves are concave downward over the whole intermediate frequency domain. This logarithmic behavior, specific to dendritic-type structures, indicates that SSWNs with $p = 0.5$ relax more slowly than those from Fig. 3(a). Even for $q = 0$ case, there is no evidence of linear chain behavior. The chains between branching points are rather short to get visible in the dynamical behavior of $G'(\omega)$. Similar findings to ours have been reported for dendrimers or some structurally disordered scale-free polymer networks [33,61,82]. Stiffness manifests strongly at small lengths scales, at rather long lengths scales its effects are reduced. For $q = 0.8$ we observe a bump in the derivative at the end of the large intermediate frequency domain. In these very short relaxation times only few monomers are involved and such large stiffness value produces strong effects. For $q = 0.6$ this bump transforms into a very short region with constant slope of $\alpha' \approx 0.22$. Of course, when stiffness increases its impact at small lengths scales get more pronounced and, in our analytical modeling, we see this through the broadening of the eigenvalue spectra. This is, also, the reason why the curves reach slower the plateau behavior when stiffness parameter grows.

Now, we turn our attention to the connections between the geometry of the SSWNs and its reflection in the relaxation dynamics described by the loss modulus, under the restrictions imposed by stiffness. Figure 4 displays the results obtained for the loss modulus, calculated based on Eq. (5) where we set $\nu k_B T/N = 1$ and $\sigma = 1$. In the left-hand side panel the stiffness parameter is set to $q = 0.4$, while in the right-hand side panel it is set to $q = 0.8$. In both panels, the randomness parameter varies from 0.01 to 0.8. In Fig. 4 we observe for all the curves a ω^1 behavior for very low frequencies and a ω^{-1} behavior for very high frequencies. In the intermediate range the topology of the networks will come into play. Again, to render the analysis more quantitative, we plot in the inset of both panels of Fig. 4 the derivative $\alpha'' = \frac{d(\log_{10} G'')}{d(\log_{10}\omega)}$ for all the curves of the main figure. In Fig. 4(a), from the behavior of the curves in the intermediate frequency domain one can easily distinguish a transition from networks with more linear segments, achieved for $p \leqslant 0.1$, to networks with highly branched architectures, obtained for $p > 0.2$. The similarity between the structures obtained for $p = 0.01$ and the pure linear chain (results denoted by circles) is evident. In the region of small intermediate frequencies the curve corresponding to $p = 0.01$ has slope value 0.47 and the linear chain has 0.5, while in the region of larger intermediate frequencies both curves have slope value 0.3. The value closer to 0.5, which is typical for fully flexible Rouse chains, relates to variability of the effective stiffness. At larger relaxation times (small frequencies) a long semiflexible chain behaves as a simple Rouse one, while at smaller relaxation times (large frequencies) it goes as $\omega^{1/4}$ [63]. For larger values of p, the curves in the intermediate frequency domain show a very pronounced dendriticlike behavior. Only for $p \geqslant 0.5$, we notice a narrow constant slope region located in the frequency interval (0.3, 10).

In comparison with Fig. 4(a), in Fig. 4(b), where $q = 0.8$, for the linear chain and for SSWNs with $p = 0.01$ the length of the intermediate frequency region where stiffness is not effective gets shortened. Instead, the length of the intermediate frequency region where stiffness is very effective gets extended. In this region $G''(\omega) \sim \omega^{0.24}$. For the networks obtained for larger values of p there is no evidence of linear chain behavior, most of the intermediate frequency domain is governed by the logarithmic behavior indicating a slowing of relaxation with the increasing of randomness parameter. At higher intermediate frequencies, the region with logarithmic behavior is followed by either a short region of constant slope $\alpha'' \approx 0.22$ for $p = 0.1$ or by a short region enclosed between two points of extreme (a local minimum and a second peak) for $p \geqslant 0.2$. This relaxation sequence between the two points of extreme gets apparent only for high q values and it is due to the gap in the eigenvalue spectrum of each network around the value of 1.0. Specifically, the gap between the closest eigenvalues of the eigenvalue 1, smaller and larger then 1.

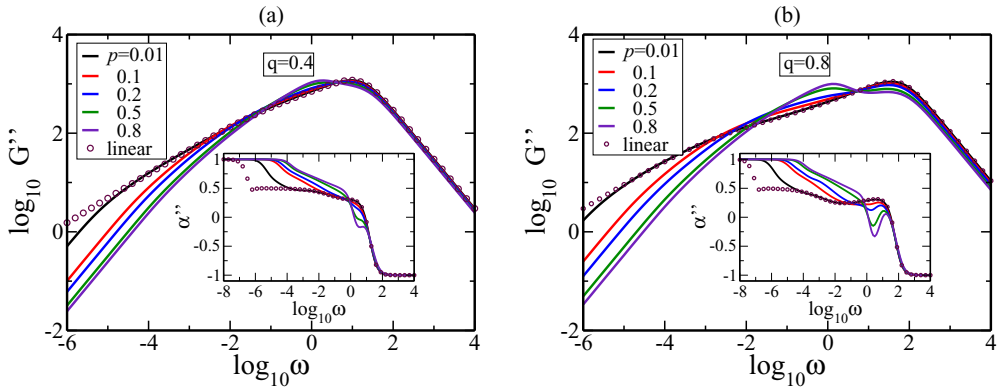

FIG. 4. Loss modulus and its derivative for SSWNs with $N = 4000$ and $S = 250$ realizations. (a) $q = 0.4$ and (b) $q = 0.8$ with p being varied.

This gap is highly dependent on stiffness parameter, a fact remarked also in the relaxation dynamics of recursive small-world polymer networks [61]. Moreover, for $p \geqslant 0.5$ the relaxation sequence presents a local minimum whose value decreases with the increase of p, but there is no significant shift on the frequency value at which the minimum appears when p is increasing. This relaxation feature is not present in Fig. 4(a) where the stiffness parameter was set to 0.4. It is worth mentioning that similar behavior has been found also for recursive small-world polymer networks [61]; however, the jumps are higher.

Our theoretical results obtained for the mechanical moduli are in good agreement with experimental rheological measurements performed on some branched polymer systems. The comparison between experimental and theoretical results concerns the scaling behavior in the intermediate frequency domain. The authors of Ref. [83] studied the linear viscoelastic response of linear ω-zwitterionic and mono-, di-, and tri-ω-zwitterionic three-arm star symmetric 1,4-polybutadienes. For some of these end-functionalized polymer melts at the reference temperature of 27°C they reported scaling exponents of 0.4, which is the value that we have obtained for SSWNs with $p = 0.1$ and $q = 0.4$. In Ref. [84], the authors investigated the rheological properties of dendronized polymers with generations 1–3 and backbone nominal degrees of polymerization in the range of 50–3000. The obtained slopes in the intermediate frequency region of the relaxation moduli range in the interval 0.5–0.7, which are similar to our findings for SSWNs with $p = 0.1$ in the frequency range $(0.001, 0.01)$ from Fig. 3(a) or for SSWNs with $p = 0.5$ in the frequency range $(0.01, 1)$ from Fig. 3(b).

C. Relaxation patterns

Figure 5 shows the results obtained for the average monomer displacement, $\langle\langle Y(t)\rangle\rangle$, calculated based on Eq. (3). In Figs. 5(a) and 5(b) we show the influence of the stiffness parameter on the motion of individual monomers and in Fig. 5(c) we show how the monomer motion is affected when bond stiffness is kept constant, but the network topology changes. In the same manner as in the previous figures, the inset graphs show the derivatives, $\alpha = \frac{d(\log_{10}\langle\langle Y\rangle\rangle)}{d(\log_{10}\omega)}$, of the curves from the main panel. Immediately apparent in all panels are the limit cases of Eq. (3), namely, in the very short times domain one has $\langle\langle Y(t)\rangle\rangle \sim t$ which is due to the diffusive motion of single beads, while at very long times one reaches $\langle\langle Y(t)\rangle\rangle \sim t/N$, which indicates that the structure moves as a whole. As before, the structure-dependent aspects are given by the intermediate time region.

In Fig. 5(a) we consider SSWNs with $p = 0.1$, meaning that linearlike segments are predominant, but there is also a quite significant number of dendritic segments. Even though the linear component is prevailing, when the parameter q is switched on, we do not observe a signature of chainlike behavior in the intermediate time range. In this subdiffusive regime, the average monomer displacement shows a logarithmic behavior which means that the network's beads move slowly due to the angular constraints on the orientations of the bonds imposed by stiffness. The curve obtained for $q = 0.8$, at the beginning of the intermediate time domain, shows a short scaling region with $\alpha \approx 0.72$. This feature can be related to the increase of the highest eigenvalues, as can be seen in Fig. 2. When bond stiffness is not considered, $\langle\langle Y(t)\rangle\rangle$ shows linear chain behavior only for a short time interval where the slope is $\alpha \approx 0.5$, the rest of the intermediate time domain being governed by the logarithmic behavior. In Fig. 5(b) we consider SSWNs with $p = 0.5$. When the angular constraints imply a branch segment its movement possibilities are fewer than those of a linear segment. In this regard, given the fact that for $p = 0.5$ the dendritic architectures prevail the network's beads move very slowly. For all employed values of q, the curves in the intermediate time domain show only logarithmic behavior. Even for $q = 0$ no power-law behavior was noticed. This result is related to the particular eigenvalue spectra, namely, there is a difference mainly in the region of high eigenvalues and there are eigenvalues with similar degeneracies, one can consider Fig. 2(b) for more details. This increase in the value of the higher eigenvalues makes the local minimum to appear for times $t \approx 1$, but it does not transform into a constant slope region as in Fig. 5(a). In Fig. 5(c) we consider SSWNs with the stiffness parameter fixed to 0.4, and we monitor the influence of the topology of the networks by varying the parameter p. The dendrimerlike behavior, more precise a logarithmic behavior, is dominant, due to the higher rate of monomers with functionality larger than 2, especially for $p > 0.2$. Even for very small values

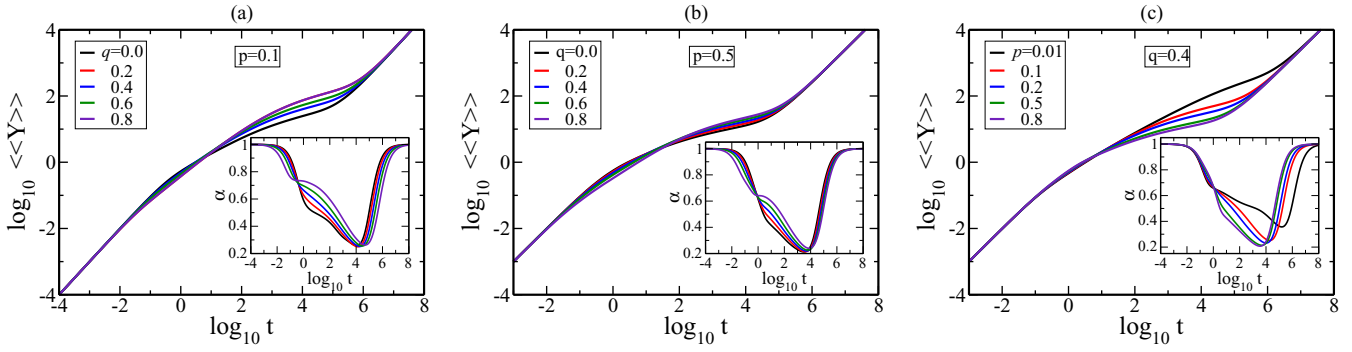

FIG. 5. Average monomer displacement and its derivative for SSWNs with $N = 4000$ and $S = 250$ realizations. (a) $p = 0.1$ and q variable, (b) $p = 0.5$ and q variable, and (c) $q = 0.4$ and p variable.

of p, such as 0.01, which corresponds to a high percentage of linearlike segments, no scaling behavior is evident in the intermediate time domain. This fact is due to the nonzero value of the stiffness parameter. For values of p equal to 0.1 and 0.2 we see a monotonous decay in the intermediate time region, while for larger values of p the decay gets narrower.

V. CONCLUSIONS

In this paper we have studied the structure properties and the relaxation dynamics of several polymer networks which were built by an algorithm that employs a degree distribution specific to small-world networks. For describing the relaxation process we have analyzed the dynamical behaviors of the average monomer displacement under locally acting forces and of the mechanical relaxation moduli. These are readily measurable quantities in rheological measurements. The analysis of the relaxation dynamics has centered on two fundamental issues: the relationship between network architecture and its dynamics and the impact of stiffness strength on the dynamical behavior of the relaxation quantities. The stiffness has been included through the correlations between bonds of a freely rotating chain, resulting an extended GGS model in which the dynamics is described by a linear set of Langevin equations coupled through a dynamical matrix. Through the employed construction algorithm, the geometry of the network is fully controlled by the randomness parameter. By increasing the randomness parameter, the resulted structures evolve from linear chains to highly branched networks through several intermediate architectures.

The eigenvalue spectra provide reliable information about the network's topology. The particular behavior of the eigenvalue spectral density as well as the degeneracy of eigenvalue 1 have allowed us to identify not only the structure topology as a whole but also that of its components. Furthermore, the bond stiffness has a strong impact on the eigenvalue spectra of the networks, namely, the highest eigenvalues increase and the lowest eigenvalues decrease by the rise of the stiffness strength. These aspects have strongly influenced the relaxation dynamics of our networks.

For the fully flexible networks obtained for low values of randomness parameter, the intermediate frequency domain of the mechanical moduli decomposes into two regions, a nonscaling region corresponding to the relaxation of the dendritic constituents followed by a scaling region corresponding to the relaxation of the linear chains. With the increase of the randomness parameter the nonscaling region increases which indicates that the dendritic shape is dominant. When the stiffness effects are considered, in the intermediate frequency domain of the mechanical moduli no linear chain behavior is evidenced, except for very small values of p corresponding to networks with highly pronounced linear character. The curves in the intermediate frequency domain follow a logarithmic behavior which indicates a slow mechanical relaxation. For the networks created based on the parameter set $(p, q) = (0.8, 0.4)$ we encountered a constant slope region, but its range is less than one order of magnitude.

In the intermediate time region of the averaged monomer displacement no linear chain behavior is noticed, apart from a very short power-law region with exponent $\alpha \approx 0.5$ obtained for $p = 0.1$ and in the absence of stiffness. The intermediate time domain of the averaged monomer displacement is ruled by logarithmic behavior, meaning that the network's beads move very slowly before the whole network starts the diffusive motion. Regarding the static properties of the networks we have noticed that for networks with the same p the mean-square radius of gyration increases with the increasing of the stiffness value, while for networks with the same stiffness value, this radius decreases with the increase of randomness parameter p.

Remarkably, our theoretical findings are well supported by mechanical relaxation experiments performed on dendronized polymers and on melts of linear and three-arm star symmetric polybutadienes. We are confident that our results can be of most interest for the experimental rheological measurements on hyperbranched semiflexible polymer networks which display a mixture of linear and (hyper)branched topology. We also hope that the recent polymer synthesis techniques [85–94], which are able to create monomers with high functionality will focus on polymer networks with our considered topology.

ACKNOWLEDGMENTS

This study was financed in part by the Coordenação de Aperfeiçoamento de Pessoal de Nível Superior-Brasil (CAPES)-Finance Code 001. A.J. gratefully acknowledges Babes-Bolyai University for financial support under Grants

No. AGC 33296/3.08.2018 and No. AGC 33297/3.08.2018. M.G. gratefully acknowledges the financial support of Brazilian agency Conselho Nacional de Desenvolvimento Cientfico e Tecnologico (CNPq).

APPENDIX A: RELAXATION DYNAMICS FOR SEMIFLEXIBLE POLYMERS

In the GGS framework, the semiflexibility is introduced by restricting the orientations of the bonds and it is modeled through the complementary interactions between the next-nearest neighboring beads. The polymer network consists of N beads, described by the set of position vectors $\mathbf{R}_i$ ($i = 1, 2, \ldots, N$), which are connected to each other by elastic springs, $\mathbf{D}_a = \mathbf{R}_i - \mathbf{R}_j$. In this model all these springs have the same elasticity constant K and obey a Gaussian statistics. The dynamics of the polymer network is described by a set of linear Langevin equations [34,36,48,52]:

$$\zeta \frac{\partial Y_i(t)}{\partial t} + \frac{\partial V_{\mathrm{STP}}(\{\mathbf{R}_k\})}{\partial Y_i} = \tilde{f}_i(t), \tag{A1}$$

where $\tilde{f}_i$ is the Y component of the usual stochastic Gaussian force acting on the ith bead, with the properties $\langle \tilde{f}(t) \rangle = 0$ and $\langle \tilde{f}_i(t)\tilde{f}_j(t') \rangle = 2k_BT\zeta\delta_{ij}\delta(t-t')$. For semiflexible polymers the bonds $\mathbf{D}_a$ are correlated, thus they are not arbitrary [61] and we can write the potential as

$$V_{\mathrm{STP}}(\{\mathbf{D}_a\}) = \frac{K}{2}\sum_{a,b} W_{ab}\mathbf{D}_a \cdot \mathbf{D}_b, \tag{A2}$$

where the K is elasticity constant and the matrix elements W_{ab} can be determined analytically, see Refs. [33,61,95,96] for more details.

The potential from Eqs. (A1) and (A2) can be expressed in terms of position vectors as

$$V_{\mathrm{STP}}(\{\mathbf{R}_k\}) = \frac{K}{2}\sum_{i,j} A^{\mathrm{STP}}_{ij}\mathbf{R}_i \cdot \mathbf{R}_j, \tag{A3}$$

where the dynamical matrix is $\mathbf{A}^{\mathrm{STP}} = \mathbf{G}\mathbf{W}\mathbf{G}^T$, with the matrix $\mathbf{G}$ being the incidence matrix [61]. The elements of $\mathbf{A}^{\mathrm{STP}} = (A^{\mathrm{STP}}_{ij})$ are known in closed form [33,61,62] as functions of functionalities and stiffness parameters; see, for instance, Eqs. (3)–(5) from Ref. [61]. In this article we consider an homogeneous stiffness situation, i.e., all junctions experience the same stiffness parameter, for which the stiffness parameter q_i of the inner bead i with functionality f_i ($f_i > 1$) equals $q_i = \frac{q}{f_i - 1}$. Here the parameter q is a real number between 0 and 1 and it will be the only parameter that controls the stiffness effect. For $q = 0$ we obtain the pure flexible polymer (no stiffness effect) while for $q = 1$ we have the complete rigid limit for all junctions. The elements of matrix $\mathbf{A}^{\mathrm{STP}}$ can be written as a function of q and they can be classified into three distinct groups with nonvanishing values [61]. First, we have the diagonal elements, which are equal to

$$A^{\mathrm{STP}}_{ii} = 1 + \frac{q^2}{(f_{i_k} - 1 + q)(1-q)} \tag{A4}$$

if i is a peripheral node, $f_i = 1$, and

$$A^{\mathrm{STP}}_{ii} = \frac{f_i}{1-q} + \sum_{i_k \in \Delta_i} \frac{q^2}{(f_{i_k} - 1 + q)(1-q)} \tag{A5}$$

if the node i has functionality $f_i > 1$. In the last equation the set Δ_i contains only the neighboring nodes i_k of node i.

In the second group we have the nondiagonal nearest-neighboring elements of matrix $\mathbf{A}^{\mathrm{STP}}$. These elements are equal to

$$A^{\mathrm{STP}}_{ii_k} = -\frac{1}{1-q} \tag{A6}$$

if either i or i_k is a peripheral bead and

$$A^{\mathrm{STP}}_{ii_k} = -\frac{1+q}{1-q} \tag{A7}$$

if both i and i_k beads have functionalities larger than 1.

The last group is formed by the nondiagonal next nearest-neighboring elements. These depend only on the functionality of bead i_k which is a common nearest neighbor of the beads i and i_{ks} and are expressed as

$$A^{\mathrm{STP}}_{ii_{ks}} = \frac{q}{(f_{i_k} - 1 + q)(1-q)}. \tag{A8}$$

The solution of Eq. (A1) is found by deploying a normal mode analysis and after averaging both over the fluctuating forces and over all the bead positions one obtains an expression that requires only the eigenvalues of the dynamical matrix $\mathbf{A}^{\mathrm{STP}}$. Thus, the average monomer displacement along the Y axis takes the following form [33,36]:

$$\langle\langle Y \rangle\rangle = \frac{2l^2K}{N\zeta}t + \frac{2l^2}{N}\sum_{n=2}^{N}\frac{1 - \exp(-K\lambda_n t/\zeta)}{\lambda_n}, \tag{A9}$$

where λ_n are the eigenvalues of $\mathbf{A}^{\mathrm{STP}}$. In this paper we considered for simplicity that $\frac{2l^2K}{\zeta} = 1$ and $2l^2 = 1$.

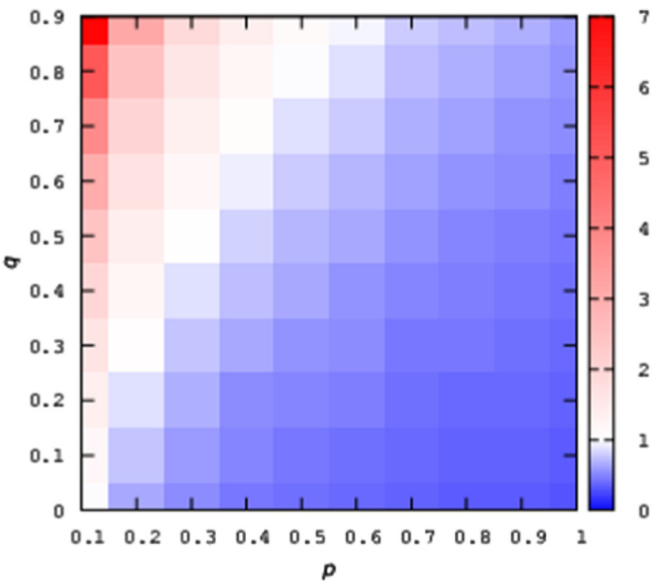

FIG. 6. Normalized radius of gyration for $S = 1000$ small-world degree-distributed treelike networks with $N = 1000$ nodes.

APPENDIX B: RADIUS OF GYRATION

A basic structural feature of a macromolecular system is its radius of gyration. In the framework of the GGS model, for both fully flexible and semiflexible polymers, the mean-squared radius of gyration which represents a measure of the size of the macromolecule can be calculated from an expression involving the sum of the reciprocal of all nonzero eigenvalues of the corresponding matrix [35,97–99]. Specifically, for the fully flexible polymers case one uses the eigenvalue spectrum of a matrix structure (connectivity matrix) describing the connectivity of the polymer; instead, for the more involved case where stiffness effects are accounted for, the same expression holds, but one uses the eigenvalues of the dynamical matrix $\mathbf{A}^{\mathrm{STP}}$. It reads as

$$R_g^2 = \frac{l^2}{N}\sum_{n=2}^{N}\frac{1}{\lambda_n}, \tag{B1}$$

where for this quantity we consider l^2 equal to 1.

In Fig. 6 we display as 2D contour plot the mean-squared radius of gyration, Eq. (B1), for networks with $N = 1000$ vertices as a function of the parameter's set (p, q). Here, the parameter p ranges between 0.1 and 1.0 and the stiffness parameter takes values from 0.0 to 0.9. We display the radius of gyration R_g^2 normalized by the the radius R_{g0}^2 calculated for the lowest considered value of p and fully flexible networks, namely, $(p, q) = (0.1, 0.0)$. In this way, one is able to visualize the contraction or the expansion of SSWNs in comparison to our reference. For a better visualization we consider a color gradient and the exact value of the radius of gyration can be mapped from the color box. Thus, the values lower than 1 stand for a contraction of the radius of gyration and the values higher than 1 correspond to an expansion. The largest value shown in the figure, $R_g^2/R_{g0}^2 = 6.89$, was found for networks with $p = 0.1$ and $q = 0.9$, which correspond to a predominant linearlike topology and the highest considered semiflexibility. We observe that for networks with the same value of p the radius of gyration increases with the increasing of the value of q, i.e., the semiflexibility expands the networks. This feature is more proeminent for networks with more linear segments (lower values of p). For networks with the same stiffness parameter q the radius of gyration continues to increase monotonously, but from high to low values of p. The highest contraction was encountered for fully flexible $(q = 0.0)$ networks with $p = 1$.

[1] L. A. N. Amaral, A. Scala, M. Barthélémy, and H. E. Stanley, Proc. Natl. Acad. Sci. USA **97**, 11149 (2000).
[2] R. Guimera, S. Mossa, A. Turtschi, and L. Amaral, Proc. Natl. Acad. Sci. USA **102**, 7794 (2005).
[3] P. Sen, S. Dasgupta, A. Chatterjee, P. A. Sreeram, G. Mukherjee, and S. S. Manna, Phys. Rev. E **67**, 036106 (2003).
[4] V. Latora and M. Marchiori, Phys. Rev. Lett. **87**, 198701 (2001).
[5] J. Lin and Y. Ban, Trans. Rev. **33**, 658 (2013).
[6] U. Alon, M. G. Surette, N. Barkai, and S. Leibler, Nature (London) **397**, 168 (1999).
[7] A. Zhang, *Protein Interaction Networks* (Cambridge University Press, Cambridge, 2009).
[8] L. F. Costa, O. N. Oliveira, Jr., G. Travieso, F. A. Rodrigues, P. R. Villas Boas, L. Antiqueira, M. P. Viana, and L. E. C. Rocha, Adv. Phys. **60**, 329 (2011).
[9] G. Bagler and S. Sinha, Physica A (Amsterdam) **346**, 27 (2005).
[10] K. Goh, M. E. Cusick, D. Valle, B. Childs, M. Vidal, and A.-L. Barabási, Proc. Natl. Acad. Sci. USA **104**, 8685 (2007).
[11] V. van Noort, B. Snel, and M. A. Huynen, EMBO Rep. **5**, 280 (2004).
[12] M. Costanzo *et al.*, Science **353**, aaf1420 (2016).
[13] E. Bullmore and O. Sporns, Nat. Rev. Neurosci. **10**, 186 (2009).
[14] S. F. Muldoon, E. W. Bridgeford, and D. S. Bassett, Sci. Rep. **6**, 22057 (2016).
[15] B. Percha, R. Dzakpasu, M. Zochowski, and J. Parent, Phys. Rev. E **72**, 031909 (2005).
[16] S. L. Pimm, J. H. Lawton, and J. E. Cohen, Nature (London) **350**, 669 (1991).
[17] J. O. Riede, B. C. Rall, C. Banasek-Richter, S. A. Navarrete, E. A. Wieters, M. C. Emmerson, U. Jacob, and U. Brose, Adv. Ecol. Res. **42**, 139 (2010).
[18] T. C. Ings *et al.*, J. Anim. Ecol. **78**, 253 (2009).
[19] T. I. Marina, L. A. Saravia, G. Cordone, V. Salinas, S. R. Doyle, and F. R. Momo, PLoS ONE **13**, e0198217 (2018).
[20] S. Wasserman and K. Faust, *Social Network Analysis* (Cambridge University Press, Cambridge, UK, 1994).
[21] M. E. J. Newman, SIAM Rev. **45**, 167 (2003).
[22] Z. Ertem, A. Veremyev, and S. Butenko, Soc. Netw. **46**, 1 (2016).
[23] L. A. Adamic, B. A. Huberman, A.-L. Barabási, R. Albert, H. Jeong, and G. Bianconi, Science **287**, 2115 (2000).
[24] T. Zhang, J. Cao, Y. Chen, L. Cuthbert, and M. Elkashlan, IEEE Commun. Lett. **17**, 1928 (2013).
[25] D. J. Watts and S. H. Strogatz, Nature (London) **393**, 440 (1998).
[26] S. Jespersen, I. M. Sokolov, and A. Blumen, J. Chem. Phys. **113**, 7652 (2000).
[27] M. E. J. Newman and D. J. Watts, Phys. Rev. E **60**, 7332 (1999).
[28] Z. Zhang, L. Rong, and C. Guo, Physica A (Amsterdam) **363**, 567 (2006).
[29] F. Comellas and M. Sampels, Physica A (Amsterdam) **309**, 231 (2002).
[30] R. Monasson, Eur. Phys. J. B **12**, 555 (1999).
[31] M. Newman, *Networks: An Introduction* (Oxford University Press, Oxford, UK, 2010).
[32] M. Galiceanu, E. S. Oliveira, and M. Dolgushev, Physica A (Amsterdam) **462**, 376 (2016).
[33] M. Galiceanu, A. Reis, and M. Dolgushev, J. Chem. Phys. **141**, 144902 (2014).
[34] A. A. Gurtovenko and A. Blumen, Adv. Polymer Sci. **182**, 171 (2005).
[35] J.-U. Sommer and A. Blumen, J. Phys. A **28**, 6669 (1995).
[36] P. Biswas, R. Kant, and A. Blumen, Macromol. Theory Simul. **9**, 56 (2000).

[37] A. Yu. Grosberg and A. R. Khokhlov, *Statistical Physics of Macromolecules* (AIP Press, New York, 1994).
[38] H. Schiessel, Phys. Rev. E **57**, 5775 (1998).
[39] P. E. Rouse, J. Chem. Phys. **21**, 1272 (1953).
[40] B. H. Zimm, J. Chem. Phys. **24**, 269 (1956).
[41] C. Cai and Z. Chen, Macromolecules **30**, 5104 (1997).
[42] A. A. Gurtovenko, Yu. Ya. Gotlib, and A. Blumen, Macromolecules **35**, 7481 (2002).
[43] A. A. Gurtovenko, D. A. Markelov, Yu. Ya. Gotlib, and A. Blumen, J. Chem. Phys. **119**, 7579 (2003).
[44] M. Galiceanu and A. Blumen, J. Chem. Phys. **127**, 134904 (2007).
[45] J. Roovers and B. Comanita, Adv. Polym. Sci. **142**, 179 (1999).
[46] F. Jasch, Ch. von Ferber, and A. Blumen, Phys. Rev. E **68**, 051106 (2003).
[47] Th. Koslowski, A. Jurjiu, and A. Blumen, Macromol. Theory Simul. **15**, 538 (2006).
[48] A. Blumen, Ch. von Ferber, A. Jurjiu, and Th. Koslowski, Macromolecules **37**, 638 (2004).
[49] A. Jurjiu and M. Galiceanu, Polymers **10**, 787 (2018).
[50] A. Jurjiu, Ch. Friedrich, and A. Blumen, Chem. Phys. **284**, 221 (2002).
[51] H. Liu and Z. Zhang, J. Chem. Phys. **138**, 114904 (2013).
[52] M. Galiceanu, Phys. Rev. E **86**, 041803 (2012).
[53] A. Jurjiu, D. Gomes Maia, Jr., and M. Galiceanu, Sci. Rep. **8**, 3731 (2018).
[54] A. Jurjiu, T. L. Biter, and F. Turcu, J. Chem. Phys. **146**, 034902 (2017).
[55] A. Jurjiu, M. Galiceanu, A. Farcasanu, L. Chiriac, and F. Turcu, J. Chem. Phys. **145**, 214901 (2016).
[56] M. Galiceanu and A. Jurjiu, J. Chem. Phys. **145**, 104901 (2016).
[57] A. Jurjiu, T. L. Biter, and F. Turcu, Polymers **9**, 245 (2017).
[58] A. Jurjiu, F. Turcu, and M. Galiceanu, Polymers **10**, 164 (2018).
[59] E. Agliari and F. Tavani, Sci. Rep. **7**, 39962 (2017).
[60] H. Liu, Y. Lin, M. Dolgushev, and Z. Zhang, Phys. Rev. E **93**, 032502 (2016).
[61] Y. Qi, M. Dolgushev, and Z. Zhang, Sci. Rep. **4**, 7576 (2014).
[62] M. Dolgushev and A. Blumen, J. Chem. Phys. **131**, 044905 (2009).
[63] M. Dolgushev and A. Blumen, Macromolecules **42**, 5378 (2009).
[64] E. D. Siggia, C. Bustamante, J. F. Marko, and S. B. Smith, Science **265**, 1599 (1994).
[65] R. Götter, K. Kroy, E. Frey, M. Bärmann, and E. Sackmann, Macromolecules **29**, 30 (1996).
[66] H. Noguchi and K. Yoshikawa, J. Chem. Phys. **109**, 5070 (1998).
[67] F. F. Abraham and D. R. Nelson, J. Phys. (France) **51**, 2653 (1990).
[68] F. Fürstenberg, M. Dolgushev, and A. Blumen, J. Chem. Phys. **136**, 154904 (2012).
[69] F. Fürstenberg, M. Dolgushev, and A. Blumen, J. Chem. Phys. **138**, 034904 (2013).
[70] M. Bixon and R. Zwanzig, J. Chem. Phys. **68**, 1896 (1978).
[71] M. Guenza and A. Perico, Macromolecules **25**, 5942 (1992).
[72] R. G. Winkler, P. Reineker, and L. Harnau, J. Chem. Phys. **101**, 8119 (1994).
[73] C. von Ferber and A. Blumen, J. Chem. Phys. **116**, 8616 (2002).
[74] A. Kumar and A. Biswas, J. Chem. Phys. **134**, 214901 (2011).
[75] J. Mielke and M. Dolgushev, Polymers **8**, 263 (2016).
[76] A. I. Amirova, O. V. Golub, I. B. Meshkov, D. A. Migulin, A. M. Muzafarov, and A. P. Filippov, Int. J. Polym. Anal. Charact. **20**, 268 (2015).
[77] D. Migulin, E. Tatarinova, I. Meshkov, G. Cherkaev, N. Vasilenko, M. Buzin, and A. Muzafarov, Polym. Int. **65**, 72 (2016).
[78] M. Doi and S. R. Edwards, *The Theory of Polymer Dynamics* (Clarendon Press, Oxford, UK, 1986).
[79] J. D. Ferry, *Viscoelastic Properties of Polymers*, 3rd ed. (John Wiley & Sons, New York, 1980).
[80] M. Rubinstein and R. Colby, *Polymer Physics* (Oxford University Press, Oxford, UK, 2003).
[81] G. Strobl, *The Physics of Polymers*, 3rd Edition (Springer-Verlag, Berlin, 2007).
[82] A. Kumar and A. Biswas, J. Chem. Phys. **137**, 124903 (2012).
[83] D. Vlassopoulos, M. Pitsikalis, and N. Hadjichristidis, Macromolecules **33**, 9740 (2000).
[84] S. Costanzo, L. F. Scherz, T. Schweizer, M. Kröger, G. Floudas, A. D. Schlüter, and D. Vlassopoulos, Macromolecules **49**, 7054 (2016).
[85] M. Sowinska and Z. Urbanczyk-Lipkowska, New J. Chem. **38**, 2168 (2014).
[86] C. Aydogan, G. Yilmaz, and Y. Yagci, Macromolecules **50**, 9115 (2017).
[87] A. Sunder, R. Mülhaupt, R. Haag, and H. Frey, Adv. Mater. **12**, 235 (2000).
[88] B. Voit and A. Lederer, Chem. Rev. **109**, 5924 (2009).
[89] C. R. Yates and W. Hayes, Eur. Polym. J. **40**, 1257 (2004).
[90] D. A. Tomalia, Adv. Polym. Sci. **261**, 321 (2013).
[91] A. Lederer and W. Burchard, *Hyperbranched Polymers: Macromolecules in Between Deterministic Linear Chains and Dendrimer Structures* (The Royal Society of Chemistry, London, UK, 2015).
[92] C. Gao and D. Yan, Prog. Polym. Sci. **29**, 183 (2004).
[93] A. P. Vogt and B. S. Sumerlin, Macromolecules **41**, 7368 (2008).
[94] S. Carter, B. Hunt, and S. Rimmer, Macromolecules **38**, 4595 (2005).
[95] M. Dolgushev, T. Guérin, A. Blumen, O. Bénichou, and R. Voituriez, J. Chem. Phys. **141**, 014901 (2014).
[96] M. L. Mansfield and W. H. Stockmayer, Macromolecules **13**, 1713 (1980).
[97] J. E. Martin and B. E. Eichinger, J. Chem. Phys. **69**, 4588 (1978).
[98] B. E. Eichinger and J. E. Martin, J. Chem. Phys. **69**, 4595 (1978).
[99] M. Dolgushev, G. Berezovska, and A. Blumen, J. Chem. Phys. **133**, 154905 (2010).